PASJ: Publ. Astron. Soc. Japan **63**, S1009–S1017, 2011 November 25

Discovery of Gas Bulk Motion in the Galaxy Cluster Abell 2256 with Suzaku

Takayuki TAMURA
Institute of Space and Astronautical Science, Japan Aerospace Exploration Agency, 3-1-1 Yoshinodai, Chuo-ku, Sagamihara 229-8510
tamura.takayuki@jaxa.jp
and
Kiyoshi HAYASHIDA, Shutaro UEDA, and Masaaki NAGAI
Department of Earth and Space Science, Graduate School of Science, Osaka University, 1-1 Machikaneyama, Toyonaka 560-0043

(Received 2011 January 31; accepted 2011 March 28)

Abstract

The results from Suzaku observations of the galaxy cluster Abell 2256 are presented. This cluster is a prototypical and well-studied merging system, exhibiting substructures both in the X-ray surface brightness and in the radial velocity distribution of member galaxies. There are main and sub components separated by 3′.5 in the sky and by about 2000 km s^{-1} in radial-velocity peaks of the member galaxies. In order to measure the Doppler shifts of iron K-shell lines from the two gas components by the Suzaku XIS, the energy scale of the instrument was carefully evaluated and found to be calibrated well. A significant shift of the radial velocity of the sub component gas with respect to that of the main cluster was detected. All three XIS sensors show the shift independently and consistently among the three. The difference is found to be 1500 ± 300 (statistical) ± 300 (systematic) km s^{-1}. The X-ray determined absolute redshifts of, and hence the difference between, the main and sub components are consistent with those of member galaxies in the optical band. The observation indicates robustly that the X-ray emitting gas is moving together with galaxies as a substructure within the cluster. These results along with other X-ray observations of gas bulk motions in merging clusters are discussed.

Key words: cosmology: large-scale structure — galaxies: clusters: individual (Abell 2256) — galaxies: intergalactic medium — X-rays: diffuse background

1. Introduction

Galaxy clusters are the largest and youngest gravitationally bound system among the hierarchical structures in the universe. Dynamical studies of cluster galaxies have revealed that some systems are still forming, and are unrelaxed. X-ray observations of the intracluster medium (ICM) have provided further evidence for mergers through spatial variations of the gas properties. Remarkably, sharp X-ray images obtained by Chandra have revealed shocks (e.g., Markevitch et al. 2002) and density discontinuities (or "cold fronts"; e.g., Vikhlinin et al. 2001). These are interpreted as various stages of on-going or advanced mergers, and suggest supersonic (for the shock) or transonic (cold front) gas motions. Cluster mergers involve a large amount of energies, and hence influence numerous kinds of observations. In particular, possible effects of gas bulk motions on the X-ray mass estimates have been investigated extensively, mostly based on numerical simulations (e.g., Evrard et al. 1996; Nagai et al. 2007). This is mainly because the cluster mass distribution is one of the most powerful tools for precise cosmology. Furthermore, cluster mergers heat the gas, develop gas turbulence, and accelerate particles, which in turn generate diffuse radio and X-ray halos.

To understand the physics of cluster mergers, gas dynamics in the system should be studied. The gas bulk motion can be measured most directly using the Doppler shift of X-ray line emission. These measurements are still challenging because of the limited energy resolutions of the current X-ray instruments. Dupke, Bregman, and their colleagues searched for bulk motions using ASCA in nearby bright clusters. They claimed detections of large-velocity gradients, such as that consistent with a circular velocity of 4100^{+2200}_{-3100} km s^{-1} (90% confidence) in the Perseus cluster (Dupke & Bregman 2001a) and that of 1600 ± 320 km s^{-1} in the Centaurus cluster[1] (Dupke & Bregman 2001b). These rotations imply a large amount of kinetic energy comparable to the ICM thermal one. Note that they used the ASCA instruments (GIS and SIS), which have gain accuracies of about 1% (or 3000 km s^{-1}). Dupke and Bregman (2006) also used Chandra data, and claimed a confirmation of the motion in the Centaurus cluster. These important results, however, have not yet been confirmed by other groups. For example, Ezawa et al. (2001) used the same GIS data of the Perseus cluster, and concluded no significant velocity gradient. In addition, Ota et al. (2007) found that the Suzaku results of the Centaurus cluster are difficult to reconcile with claims in Dupke and Bregman (2001b, 2006). In short, previous results by Dupke and Bregman suggest bulk motions in some clusters, but with large uncertainties.

Currently the Suzaku XIS (Koyama et al. 2007a) would be the best X-ray spectrometer for a bulk-motion search, because of its good sensitivity and calibration (Ozawa et al. 2009). In fact, Suzaku XIS data were already used for this search in representative clusters. Tight upper limits on velocity variations are reported from the Centaurus cluster (1400 km s^{-1};

[1] The error confidence range is not explicitly mentioned in the reference.

Table 1. Fitting parameters of the radial-velocity distribution of member galaxies.

Component number in the reference	Mean velocity (km s^{-1})	Dispersion (km s^{-1})
Briel et al. (1991)		
1 (main)	17880 ± 205	1270 ± 127
2 (sub)	15730 ± 158	350 ± 123
Berrington, Lugger, and Cohn (2002)*		
1 (53 galaxies; sub)	15700	550
2 (196 galaxies; main)	17700	840
3 (28 galaxies)	19700	300

* Errors on velocities and dispersions are not given in the paper.

90% confidence; Ota et al. 2007) and A 2319 (2000 km s^{-1}; 90% confidence; Sugawara et al. 2009) among others.

In order to improve the accuracy of the velocity determination, and to search for gas bulk motions, we analyzed Suzaku XIS spectra of the Abell 2256 cluster of galaxies (A 2256, redshift of 0.058). This X-ray bright cluster is one of the first systems showing substructures not only in the X-ray surface brightness, but also in the galaxy velocity distribution (Briel et al. 1991). In the cluster central region, there are two systems separated by 3′.5 in the sky. Motivated by this double-peaked structure in their Rosat image, Briel et al. (1991) integrated the velocity distribution of galaxies from Fabricant et al. (1989) over the cluster, fitted it to two Gaussians, and found two separated peaks in the velocity distribution. The two structures are separated by ~ 2000 km s^{-1} in radial-velocity peaks of member galaxies, as given by table 1. Berrington, Lugger, and Cohn (2002) added new velocity data to the Fabricant, Kent, and Kurtz (1989) sample, used 277 member galaxies in total, and confirmed the two systems along with an additional third component (table 1). This unique finding motivated subsequent observations in multiple wavelengths. For example, radio observations revealed a diffuse halo, relics, and tailed radio emission from member galaxies (e.g., Röttgering et al. 1994). The Chandra observation by Sun et al. (2002) revealed detailed gas structures in and around the main and second peaks. Furthermore, there are some attempts to reproduce merger history of A 2256 using numerical simulations (e.g., Roettiger et al. 1995). Thus, A 2256 is a prototypical and well-studied merging system, and is hence suitable to study the gas dynamics.

We carefully evaluated instrumental energy scales of the Suzaku XIS, used iron K-shell line emission, and found a radial-velocity shift of the second gas component with respect to the main cluster. The X-ray determined redshifts are consistent with those of galaxy components. This is the most robust detection of a gas bulk motion in a cluster.

Throughout this paper, we assume cosmological parameters as follows: $H_0 = 70$ km s^{-1} Mpc^{-1}, $\Omega_{\rm m} = 0.3$, and $\Omega_\Lambda = 0.7$. At a cluster redshift of 0.058, one arc-minute corresponds to 67.4 kpc. We use the 68% ($1\,\sigma$) confidence level for errors, unless stated otherwise.

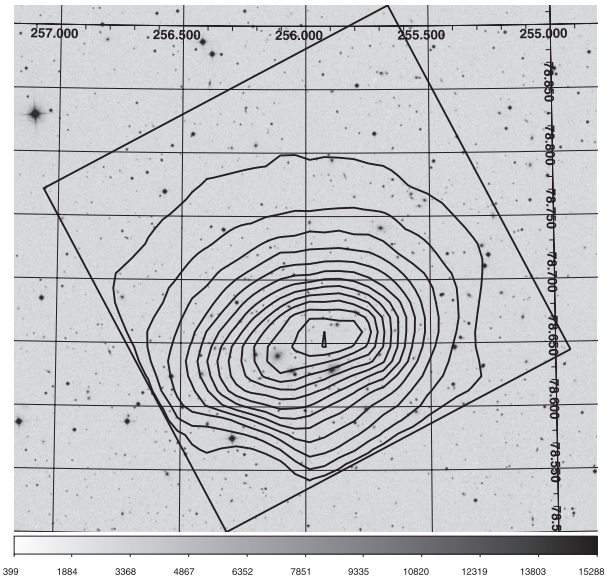

Fig. 1. Suzaku XIS contour image of A 2256 in the 0.3–10 keV band overlaid on a DSS (Digital Sky Survey by the Space Telescope Science Institute) optical image. The three XIS data are co-added. The XIS field of view is shown by a square. The contour levels are linear from 10 to 160 counts pixel^{-1}. No vignetting nor background was corrected. The calibration-source regions at corners of CCD are excluded. North is up and east is to left.

2. Observations

Suzaku observations of A 2256 were performed on 2006 November 10–13 (PI: K. Hayashida). The XIS was in the normal window and the spaced-row charge injection off modes. The observation log is given in table 2. Figure 1 shows an X-ray image of the cluster. Detailed descriptions of the Suzaku observatory, the XIS instrument, and the X-ray telescope are found in Mitsuda et al. (2007), Koyama et al. (2007a), Serlemitsos et al. (2007), respectively.

To verify the XIS gain calibration, we have also used data from the Perseus cluster observed in 2006 with the same XIS modes as those for A 2256 (table 2). These data had already been used for the XIS calibration (e.g., Ozawa et al. 2009) and scientific analyses (Tamura et al. 2009; Nishino et al. 2010).

3. Analysis and Results

3.1. Data Reduction

We used version 2.1 processing data along with the HEASOFT version 6.9. In addition to the XIS standard event selection criteria, we screened data by adding the following conditions: geomagnetic cut-off-rigidity, > 6 GV; elevation angle above the sunlit Earth, $> 20°$, and dark Earth, $> 5°$. We used the latest calibration file as of 2010 July. Using these files, we corrected the XIS energy scale. The data from three CCDs (XIS 0, XIS 1, and XIS 3) were used.

We examined the light curve excluding the central bright-region events ($R < 6'$) for stable-background periods. There was no flaring event in the data. The instrumental (non-X-ray) background was estimated using the night-Earth observation

Table 2. Suzaku observations of A 2256 and the Perseus cluster.

Target	Date	Sequence number	(RA, Dec) (°, J2000.0)	*PA** (°)	Net exposure (ks)
A 2256	2006/11/10–13	801061010	(256.0138, 78.7112)	208	94.4
Perseus	2006/02/01	800010010	(49.9436, 41.5175)	260	43.7
Perseus	2006/08/29	101012010	(49.9554, 41.5039)	66	46.6

* The nominal position angle (north to DETY axis).

database and the software xisnxbgen (Tawa et al. 2008).

We prepared X-ray telescope and CCD response functions for each spectrum using the software xissimarfgen (Ishisaki et al. 2007) and xisrmfgen (Ishisaki et al. 2007), respectively. The energy bin size is 2 eV.

To describe the thermal emission from a collisional ionization equilibrium (CIE) plasma, we used the APEC model (Smith et al. 2001) with the solar metal abundances taken from Anders and Grevesse (1989).

3.2. *Energy Scale Calibration*

The main purpose of this paper is to describe our measurement of the Doppler shifts of K-shell iron lines in X-ray. In these analyses, the energy-scale calibration is crucial. In sub-subsection 3.2.1, we summarize the calibration status. In sub-subsection 3.2.2, we attempt to confirm the calibration using calibration-source data collected during the A 2256 observation. The primal goal here is to find differences of line energies observed at different positions within the field of view. Therefore, the positional dependence of the energy scale is most important, which is described in subsubsection 3.2.3. Here, we focus on data obtained in the spaced-row charge-injection off mode and around the K-shell iron lines. Considering all of the available information given here, as summarized in table 3, we assume that the systematic uncertainty of the energy scale around the iron lines is most likely 0.1% and 0.2% at most over the central $14'.7 \times 14'.7$ region or among the three CCDs.

3.2.1. *Reported status*

Koyama et al. (2007b) estimated the systematic uncertainty of the absolute energy in the iron band to be within $+0.1\%, -0.05\%$, based on the observed lines from the Galactic center along with the Mn Kα and Kβ lines (at 5895 eV and 6490 eV respectively) from the built-in calibration source (^{55}Fe). Independently, Ota et al. (2007) investigated the XIS data of two bright and extended sources (the A 1060 and Perseus clusters), and evaluated the positional energy-scale calibration in detail. They estimated the systematic error of the spatial gain non-uniformity to be $\pm 0.13\%$. Furthermore, Ozawa et al. (2009) systematically examined the XIS data obtained from the start of operation in 2005 July until 2006 December. They reported that the position dependence of the energy scale is well corrected for the charge-transfer inefficiency, and that the time-averaged uncertainty of the absolute energy is $\pm 0.1\%$. In addition, the gradual change of the energy resolution was also calibrated; the typical uncertainty of resolutions is 10–20 eV in full width-half maximum.

3.2.2. *Absolute scale*

We extracted spectra of calibration sources that illuminate two corners of each CCD (segments A and D). These spectra in the energy range of 5.3–7.0 keV were fitted with two Gaussian lines for the Mn Kα and Kβ along with a bremsstrahlung continuum component. Here, we fixed the energy ratio between the two lines to the expected one. The thus-obtained energy centroids of the Mn Kα line from the two corners of three CCDs give an average of 5904 eV (as compared with the expected value of 5895 eV) and a standard deviation (scatter among the six centroids) of 6 eV. The statistical errors of the line center were about 1–2 eV. This confirms that the absolute energy scale averaged over all CCDs and the relative gain among CCD segments are within $\pm 0.15\%$ and $\pm 0.10\%$, respectively. Simultaneously, we found that the data could be fitted with no intrinsic line width for the Gaussian components, meaning that the energy resolution was also well calibrated.

3.2.3. *Spatial variation*

We used the XIS data of the Perseus cluster, which would provide the highest-quality XIS line spectra over the whole CCD field of view among all of the Suzaku observations. Here, we assume no line shift intrinsic to the cluster within the observed region. There were two exposures of Perseus in the normal window and the spaced-row charge injection off modes (table 2) in periods close to the A 2256 observation. Note that Ota et al. (2007) used the same data, but with early calibration (i.e., version 0.7 data). Here, we re-examine the accuracy with the latest and improved calibration.

Firstly, following Ota et al. (2007), we divided the XIS field of view into 8×8 cells of size $2'.1 \times 2'.1$. Each spectra in the 6.2–7.0 keV band was fitted with two Gaussian lines for He-like Kα ($\sim$6700 eV) and H-like Kα ($\sim$6966 eV) and a bremsstrahlung continuum model. Here, we fixed the ratio of the central energies between the two lines to a model value of 1.040, and let the energy of the first line be a fitting parameter. Because of the low-statistics data in CCD peripheral regions we focused on the central 7×7 cells (i.e., $14'.7 \times 14'.7$). The typical statistical errors of the line energy were from ± 4 eV to ± 25 eV. Thus, the derived central energies from 7×7 cells for each CCD were used to derive an average and a standard deviation. The average values were 6575 eV, 6575 eV, and 6569 eV, for XIS 0, XIS 1, and XIS 3, respectively, which are consistent with the cluster redshift of 0.017–0.018. The standard deviations among 7×7 cells were 7 eV, 13 eV, and 10 eV for the three CCDs, respectively. There was no cell having a significant deviation from the average value at more than the 2σ level. These deviations include not only systematics due to the instrumental gain uncertainty, but also statistics and

Table 3. Accuracy of the XIS energy scale calibration and the observed velocity shift.

Section*	Line used	$\Delta^{\dagger}$ (%)	Reference and remarks
3.2.1	GCDX/Fe-K‡	$+0.1$, -0.05	Koyama et al. (2007b); uncertainty of the absolute energy.
3.2.1	Perseus/Fe-K	± 0.13	Ota et al. (2007); spatial non-uniformity (at 68% confidence).
3.2.1	Mn I Kα	± 0.1	Ozawa et al. (2009); time-averaged uncertainty of the absolute energy.
3.2.2	Mn I Kα	± 0.10	This paper; standard deviation among CCD segments in the A 2256 data.
3.2.3	Perseus/Fe-K	$+0.06$, -0.09	This paper; variations between the two regions.
3.4	A 2256/Fe-K	0.5 ± 0.1	This paper; velocity shift in A 2256, after correcting the inter-CCD gain and the statistical error.

* Sub-subsection/subsection number in this paper.
† Possible uncertainty, velocity shift, or its error all in percentage of the line energy. At the iron K line, 0.1% corresponds to 7 eV for the energy shift or 300 km s^{-1} for the radial velocity.
‡ From the Galactic center diffuse emission.

systematics intrinsic to the Perseus emission. Therefore, the energy scale uncertainty should be smaller than this range of deviations (0.1%–0.2%).

Secondly, we focus on the CCD regions specific in our analysis below. We extracted the Perseus spectra from the same detector regions (main and sub) as used in the A 2256 analysis. The definitions of the regions are given in figure 2 and subsection 3.4. These spectra were fitted with the same model as above and used to derive the redshift (from the line centroid). We found no difference in the redshift between the two regions. The redshift differences (between the two regions from the three sensors) ranged from -9×10^{-4} to $+6 \times 10^{-4}$ with an average of 1.5×10^{-5}. Accordingly, we estimated the possible instrumental gain shift to be within $\pm 0.10\%$ with no systematic bias between the two regions.

3.3. *Energy Sorted X-Ray Images*

In order to examine the spectral variation over the A 2256 central region, we extracted two images in different energy bands including He-like and H-like iron line emissions, as shown in figure 2. There appear at least two emission components that correspond to the main cluster at east and the sub component at west discovered in Briel et al. (1991). We noticed a clear difference in the distribution between the two images. In the He-like iron image, the sub component exhibits brightness comparable to that of the main component. On the other hand, in the H-like iron image, the sub has lower brightness. This clearly indicates that the sub has cooler emission compared with the main. Based on these contrasting spatial distributions, we define the centers of the two components to be (256.°1208, 78.°6431) and (255.°7958, 78.°6611), in equatorial J2000.0 coordinates (RA, Dec), respectively, as shown in figure 2.

3.4. *Radial Velocity Shift*

3.4.1. *Separate spectral fitting*

Our goal is to constrain the velocity shift of the sub component with respect to the main cluster. We then extracted sets of spectra from the two components, and fitted them with different redshifts. More specifically, for the main-component emission, we integrated the data within $4'$ in radius from the main center, but excluding a sub-component region with a radius of $2'$ (figure 2). For the sub region, data within $1'.5$ in radius from the sub center were extracted.

Table 4. Spectral-fitting results from the main and sub regions.

Region	kT (keV)	Fe (solar)	$\langle z \rangle$*	χ^2/d.o.f.
FIT-1, CIE component				
Main	7.1 ± 0.3	0.25 ± 0.02	0.0583	121/139
Sub	5.0 ± 0.4	0.29 ± 0.03	0.0528	135/139
FIT-2, two Gaussian components				
Main	6.2 ± 0.7	—	0.0580	112/137
Sub	4.5 ± 0.9	—	0.0528	131/137
FIT-3, two Gaussians with the gain correction				
Main	6.2 ± 0.7	—	0.0590 ± 0.0007	118/137
Sub	4.6 ± 0.9	—	0.0540 ± 0.0005	137/137

* Average value over three CCD data for the FIT-1 and FIT-2 is given. Statistical errors on these values are typically 0.001. In the FIT-3, a single redshift common to the three CCDs is assumed.

We used the energy range of 5.5–7.3 keV around the iron line complex. In this energy band the cosmic background fluxes were below a few percent of the source count in the two regions. Therefore we ignored this background contribution.

We used a CIE component to model the spectra. The free parameters were an iron line redshift, the temperature, the iron abundance, and normalization. Models for the three CCDs were assumed to have different redshifts and normalizations to compensate for any inter-CCD calibration uncertainties. Other parameters, temperature and abundance, were fixed to be common among the CCDs. As shown in figure 3 and table 4, these models describe the data well (FIT-1). The fits give different redshifts between the two regions from all three CCDs, as shown in figure 4a. The statistical errors of the absolute redshift are less than ± 0.002. The redshift differences between the two regions are 0.0048, 0.0041, and 0.0076 for the three CCDs. These are equivalent to shifts of 30–50 eV in energy or 1200–2300 km s^{-1} in radial velocity.

The spectral shape of the two regions are different, as shown in figure 3. Therefore, the obtained redshift difference may depend on the spectral modeling. To check this possibility, instead of the CIE model, we used two Gaussian lines and

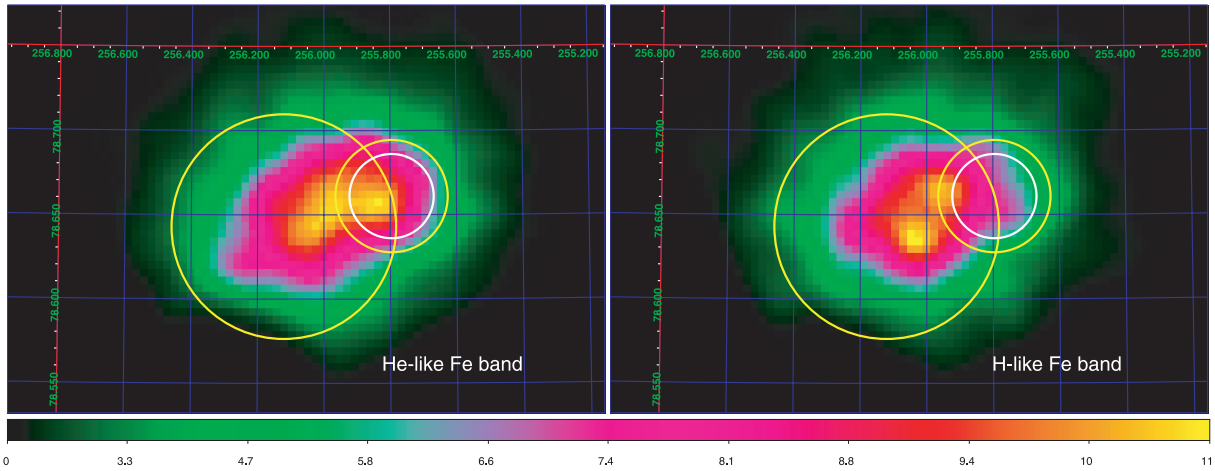

Fig. 2. XIS images of A 2256 from the 6.10–6.48 keV energy band including He-like iron emission (left) and from the 6.48–6.80 keV band including H-like iron emission (right) in units of counts. No vignetting nor background was corrected. Images have been smoothed with a Gaussian filter with $\sigma = 17''$. The spectra are extracted from the two regions indicated by circles in yellow (the main region) and a circle in white (the sub; the details are described in sub-subsection 3.4.1.).

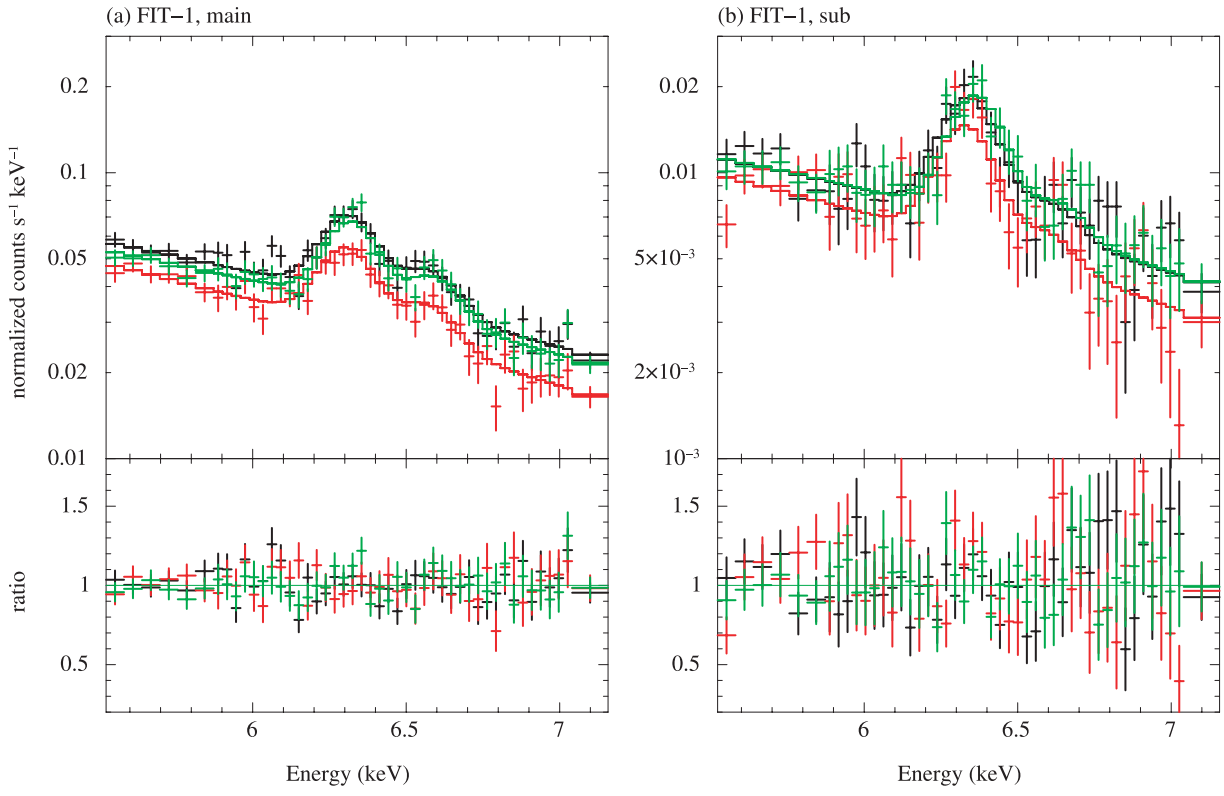

Fig. 3. Cluster spectra along with the best-fit CIE model in histogram (FIT-1). Plots (a) and (b) are from the main and sub regions, respectively. The XIS 0, XIS 1, and XIS 3 data are shown by black, red, and green colors, respectively. In the lower panels, the fit residuals in terms of the data to model ratio are shown.

a bremsstrahlung continuum component (FIT-2). Here, we assumed the He-like iron resonance line centered on 6682 eV and the H-like iron Lyα centered on 6965 eV for the two lines, and determined the redshift common to these two lines. The Gaussian components were set to have no intrinsic width. As given in table 4, these models give slightly better fits to the data in general than the first model. For each CCD, we obtained redshifts (and therefore a redshift difference) the same as those from the first fit within the statistical uncertainty. Therefore, the redshift depends insignificantly on the spectral modeling.

Strictly speaking line centroids of the iron line transitions could change depending on the emission temperature. In the case of the observed region of A 2256, where the temperature varies within 4–8 keV (e.g., Sun et al. 2002), the strong iron line structure is dominated by the He-like triplet. Within this temperature range, the emission centroid of the triplet stays

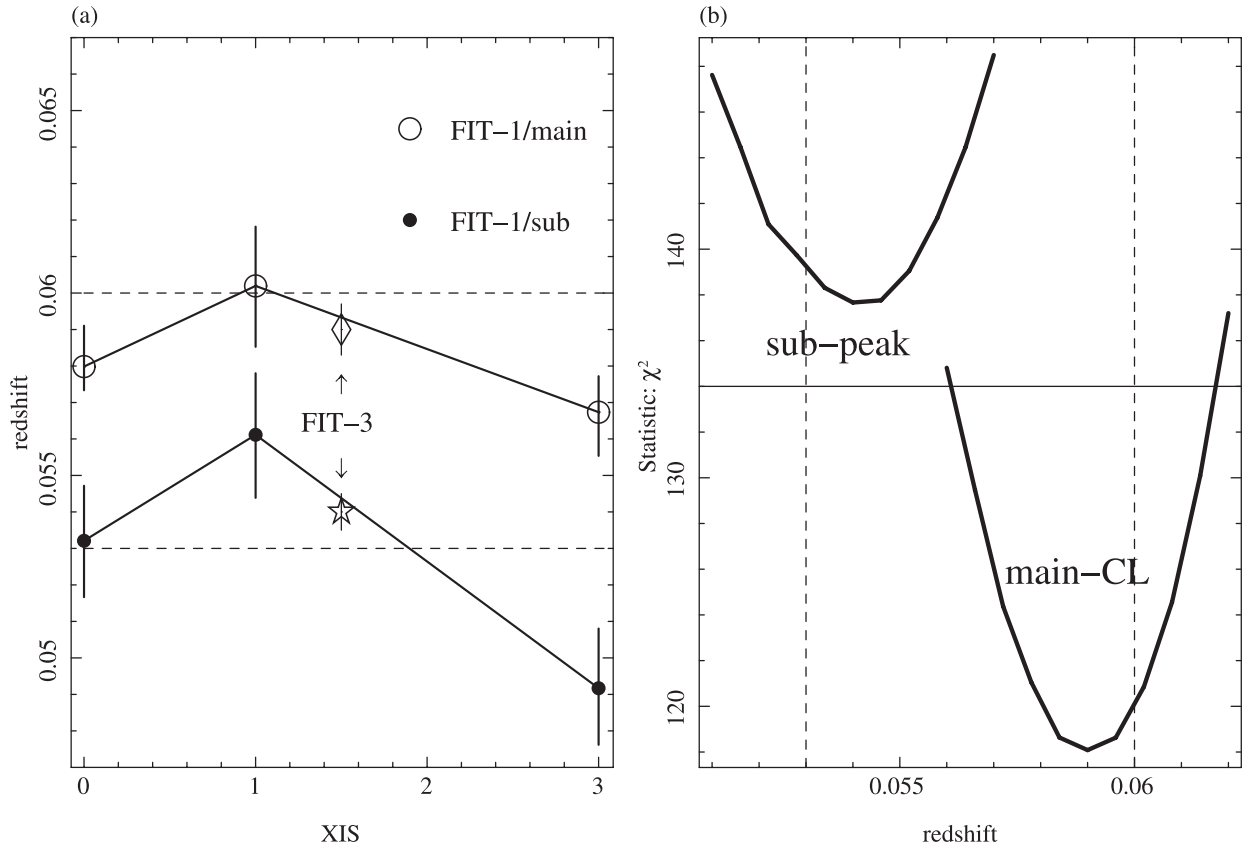

Fig. 4. (a) Redshifts obtained from the CIE fitting (FIT-1) of the main and sub component regions for each CCD (X-axis). The gain-corrected results of FIT-3 are shown at the position of XIS = 1.5. The two horizontal dashed lines indicate redshifts from the optical data (Briel et al. 1991; table 1). (b) Statistic χ^2 distributions of the gain-corrected Gaussian fitting (FIT-3) of the two regions as a function of the redshift. The horizontal line at $\chi^2 = 134$ indicates the degree of freedom of the fits. The two vertical dashed lines indicate the redshifts as in (a).

within 6682–6684 eV based on the APEC model. This possible shift (< 2 eV) is well below the obtained redshift difference (30–50 eV) and should not be the main origin of the difference.

3.4.2. Gain-corrected spectral fitting

The obtained redshifts are systematically different among the three CCDs (figure 4a). We attempt to correct this inter-CCD gain difference based on the calibration source data. Following Fujita et al. (2008), we estimated the gain correction factor, $f_{\rm gain}$, by dividing the obtained energy of the Mn K line from the calibration source by the expected one. In the A 2256 data, as given in subsection 3.2, $f_{\rm gain}$ are 1.0018 (XIS 0), 1.0000 (XIS 1), and 1.0016 (XIS 3). This factor, the redshift obtained from the fit ($z_{\rm fit}$), and the corrected redshift ($z_{\rm cor}$) have the relation

$$f_{\rm gain} = \frac{z_{\rm cor} + 1}{z_{\rm fit} + 1}. \quad (1)$$

We used this correction and fit the spectra with a single redshift common to the three CCDs to the two-Gaussian model (FIT-3). These models gave slightly poorer fits compared with the previous ones, because of a decrease in the degree of freedom (table 4). Nevertheless, the fits are still acceptable. The difference in the redshift between the two regions is 0.005 ± 0.0008 (or $1500 \pm 240\,{\rm km\,s^{-1}}$). In figure 4b we show the statistical χ^2 distribution as a function of the redshift. This clearly indicates that the data cannot be described by the same redshift for the main and sub regions.

We found that the redshifts determined here by X-rays are consistent with those of member galaxies in the optical region (table 1), as explained below. The X-ray redshift of the main component, $z = 0.0590$ or $17700\,{\rm km\,s^{-1}}$, is the same as the galaxy redshift within the statistical error. That of the sub component, $z = 0.0540$ or $16200\,{\rm km\,s^{-1}}$, is larger than the galaxy value of $15730\,{\rm km\,s^{-1}}$. Yet, the difference, $470\,{\rm km\,s^{-1}}$, is within the combined errors from X-ray statistical ($150\,{\rm km\,s^{-1}}$), systematic ($300\,{\rm km\,s^{-1}}$), and optical fitting ($160\,{\rm km\,s^{-1}}$). Besides this, the obtained spectra of the sub component could be contaminated from the emission of the main component due to the projection and the telescope point spread function (half power diameter of about 2′). This contamination could make the obtained redshift of the sub larger than the true one (or closer to that of the main).

To visualize the redshift shift in the sub region more directly, we show spectral fittings by combining the two front-illuminated CCDs (XIS 0 and 3) data in figure 5. We fitted the spectra with the two Gaussians model, as given above. In this figure we compare the fitting results between the best-fit model ($z = 0.051$) and one with the redshift fixed to the main cluster

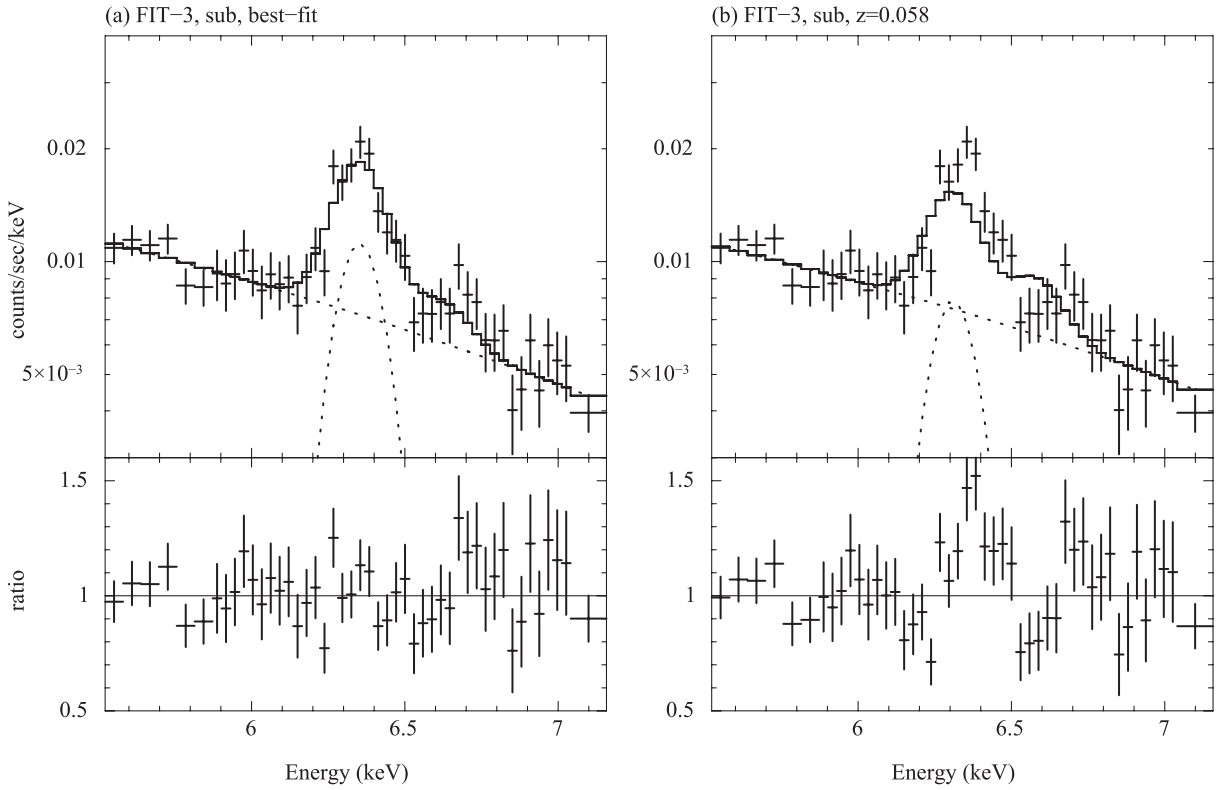

Fig. 5. Spectra from the sub-component region by adding the two front-illuminated CCDs (XIS 0 and 3), fitted with two Gaussians and a continuum model. (a) Redshift common to the two lines is left free. The model gives the best-fit redshift of 0.05115 and χ^2 of 40.4 for a degree of freedom of 42. (b) Redshift is fixed to the main component value ($z = 0.058$). The model gives χ^2 of 80.8 for a degree of freedom of 43.

value ($z = 0.058$). This comparison shows that we can reject that the sub region has the same redshift as the main cluster.

4. Summary and Discussion

4.1. Summary of the Result

We found gas bulk motion of the second component in A 2256. The difference in the redshifts, and hence the radial velocities between the main and sub systems is found to be 1500 ± 300 (statistical) ± 300 (systematic) $\mathrm{km\,s^{-1}}$ (subsection 3.4). This observed shift corresponds to only 0.5% in energy, but is well beyond the accuracy of the energy scale reported by the instrument team (Koyama et al. 2007b; Ozawa et al. 2009) and that by Ota et al. (2007). Focusing on the present analysis of A 2256, we also examined the calibration systematics independently, and confirmed the accuracy given above. The obtained redshifts, and hence the difference between the two X-ray emitting gas components are consistent with those of the radial-velocity distribution in member galaxies. This consistency uniquely strengthens the reliability of our X-ray measurement.

This is the first detection of gas bulk motion not only in A 2256, but also from Suzaku, which presumably has the best X-ray spectrometer in operation for the velocity measurement. As given in section 1, Dupke and Bregman (2001a, 2001b, 2006) previously claimed detections of bulk motions in the Perseus and Centaurus clusters. Compared with these and other attempts, our measurement is more accurate and robust. This improvement is not only due to the better sensitivity and calibration of the XIS, but also due to the well-separated and X-ray bright nature of the structure in A 2256.

Radial-velocity distributions of cluster galaxies were used to evaluate the dynamics of cluster mergers. These studies, however, have limited capability. First, largely because of the finite number of galaxies and the projection effect, a galaxy sub group within a main cluster is not straightforward to identify. Second, the major baryon in the cluster is not galaxies, but the gas in most systems. Therefore, the dynamical energy in the hot gas cannot be ignored. Third, galaxies and gas are not necessary to move together, especially during the merging phases, because of the different nature of the two (collisionless galaxies and collisional gas). In practice, some clusters under the violent merging phase, such as 1E 0657−558 (Clowe et al. 2006) and A 754 (Markevitch et al. 2003), show a spatial separation between the galaxy and gas distributions. Therefore, it is important to measure the dynamics of galaxies and gas simultaneously. The present result is one of the first such attempts.

4.2. Dynamics of A 2256

The determined radial velocity, $v_r \sim 1500\,\mathrm{km\,s^{-1}}$, gives a lower limit of a three-dimensional true velocity, $v = v_r/\sin\alpha$, where α denotes the angle between the motion and the plane of the sky. Given a gas temperature of 5 keV (subsection 3.4) and an equivalent sound speed of $1100\,\mathrm{km\,s^{-1}}$ around the sub component, this velocity corresponds to a Mach number of $M > 1.4$. Therefore, at least around the sub component, the gas

kinematic pressure (or energy) can be $(1.4)^2 \sim 2$-times larger than the thermal one. In this environment, the gas departs from hydrostatic equilibrium. Then, does this motion affect the estimation of the mass of the primary cluster ? As argued by Markevitch and Vikhlinin (1997), it depends on the physical separation between the two components. In the case of A 2256, the two are not likely to be too closely connected to disturb the hydrostatic condition around the primary, as estimated below. However, to weight the total mass within the larger volume, including the sub component, we should consider not only the mass of the sub, itself, but also the dynamical pressure associated with the relative motion. This kind of a departure from hydrostatic equilibrium was generally predicted at cluster outer regions in numerical simulations (e.g., Evrard et al. 1996).

We will compare our measurement with other studies on the ICM dynamics. Markevitch et al. (2002) discovered a bow shock in the Chandra image of 1E 0657−56 (the bullet cluster), and estimated its M to be 3.0 ± 0.4 ($4700\,\mathrm{km\,s^{-1}}$) based on the observed density jump under the shock-front condition. Using a similar analysis, Markevitch et al. (2005) derived an M of 2.1 ± 0.4 ($2300\,\mathrm{km\,s^{-1}}$) in A 520. Based on a more specific configuration in the "cold front" in A 3367, Vikhlinin, Markevitch, and Murray (2001) estimated its M to be 1.0 ± 0.2 ($1400\,\mathrm{km\,s^{-1}}$). In these cases, velocity directions are assumed to be in the plane of the sky. See Markevitch and Vikhlinin (2007) for a detailed discussion and other examples. These measurements are unique, but require certain configurations of the collision to apply to observations. In contrast, X-ray Doppler-shift measurements as given in the present paper are more direct and commonly applicable to merging systems. This method is sensitive to the motion parallel to the line of sight. These two measurements are complementary, and could provide a direct measurement of three-dimensional motion if applied to a merging system simultaneously.

We measured the gas velocity parallel to the line of sight (v_r). How about the velocity in the plane of the sky (v_{sky}) and the true velocity, v? The Rosat X-ray image of A 2256 shows a steeper brightness gradient between the main and second components (Briel et al. 1991). Furthermore, from the Chandra spectroscopic data, Sun et al. (2002) found a hint of a temperature jump across the two components. They argued a similarity of this feature to the "cold front" discovered in other clusters. The temperature, and hence pressure jump, in A 2256 (from about 4.5 keV to 8.5 keV) are similar to those found in A 3367, in which the jump indicates a gas motion with v_{sky} of about $1400\,\mathrm{km\,s^{-1}}$. Therefore, we expect a similar v_{sky} in A 2256, which is comparable to v_r. Further assuming that the second component directs to the main cluster center, v is estimated to be $\sqrt{v_r^2 + v_{\mathrm{sky}}^2} \sim \sqrt{2} v_r \sim 2000\,\mathrm{km\,s^{-1}}$. Instead of assuming v_{sky}, by considering the mean $\sin\alpha$ factor, $2/\pi$, v becomes $2400\,\mathrm{km\,s^{-1}}$ on average. Based on a simple assumption that the two system started to collide from rest, we can estimate the velocity as $v \sim (2GM/R)^{1/2}$, where G, M, and R are the gravitational constant, the total mass of the system, and the separation, respectively. The total mass of A 2256 of $8 \times 10^{14}\ M_\odot$ (Markevitch & Vikhlinin 1997) and an assumed final separation R of 1 Mpc give $v \sim 2800\,\mathrm{km\,s^{-1}}$, which is comparable to, but larger than, the estimated current velocity. Putting $v = 2000$–$2400\,\mathrm{km\,s^{-1}}$ to the relation, we obtain a current separation R of 1.4–2 Mpc. The time to the final collision can be estimated to be about 0.2–0.4 Gyr [$(R - 1)$ Mpc divided by v]. Here, we assume that the system is going to the final collision. This assumption is consistent with a lack of evidence for strong disturbances in the X-ray structure, as argued previously for A 2256 in general.

4.3. *Future Prospect*

Our observations provided the first detection of gas bulk motion in a cluster. To understand in general cluster formation, which is dominated by non-linear processes, systematic measurements in a sample of clusters are required. For example, some clusters, such as 1E 0657−558 (Clowe et al. 2006) at violent merging stages, show segregation of the gas from the galaxy, and possibility from dark-matter components. In these systems, we expect different situations in the gas and galaxy dynamics compared with that found in A 2256. Given capabilities of current X-ray instruments, such as the Suzaku XIS, A 2256 is presumably a unique target with X-ray flux high and the velocity separation clear enough to resolve the structure. Accordingly, the systematic study requires new instruments with higher spectral resolutions and sufficient sensitivities. In fact, this kind of assessment is one of the primary goals for planned X-ray instruments, such as SXS (Mitsuda et al. 2010) onboard ASTRO-H (Takahashi et al. 2010). Using the SXS with an energy resolution better than 7 eV we could measure gas bulk motions in a fair number of X-ray bright clusters. Furthermore, we may find that line broadening originated from the gas turbulence, as a result of mergers, related shocks, or some activities in the massive black hole at cluster centers. In addition, the SXS potentially will constrain for the first time the line broadening from the thermal motion of ions (and hence the ion temperature). The present result proves that A 2256 is one of the prime targets for ASTRO-H. The expected spectra of the two components in A 2256 with the SXS are shown in figure 11 of Takahashi et al. (2010).

We thank the referee for useful comments. We also thank all Suzaku team members for their support. To analyze the data, we used the ISAS Analysis Servers provided by ISAS/C-SODA. KH acknowledges support by a Grant-in-Aid for Scientific Research, No. 21659292 from MEXT.

References

Anders, E., & Grevesse, N. 1989, Geochim. et Cosmochim. Acta, 53, 197
Berrington, R. C., Lugger, P. M., & Cohn, H. N. 2002, AJ, 123, 2261
Briel, U. G., et al. 1991, A&A, 246, L10
Clowe, D., Bradač, M., Gonzalez, A. H., Markevitch, M., Randall, S. W., Jones, C., & Zaritsky, D. 2006, ApJ, 648, L109
Dupke, R. A., & Bregman, J. N. 2001a, ApJ, 547, 705
Dupke, R. A., & Bregman, J. N. 2001b, ApJ, 562, 266

Dupke, R. A., & Bregman, J. N. 2006, ApJ, 639, 781
Evrard, A. E., Metzler, C. A., & Navarro, J. F. 1996, ApJ, 469, 494
Ezawa, H., et al. 2001, PASJ, 53, 595
Fabricant, D. G., Kent, S. M., & Kurtz, M. J. 1989, ApJ, 336, 77
Fujita, Y., et al. 2008, PASJ, 60, 1133
Ishisaki, Y., et al. 2007, PASJ, 59, S113
Koyama, K., et al. 2007a, PASJ, 59, S23
Koyama, K., et al. 2007b, PASJ, 59, S245
Markevitch, M., et al. 2003, ApJ, 586, L19
Markevitch, M., Gonzalez, A. H., David, L., Vikhlinin, A., Murray, S., Forman, W., Jones, C., & Tucker, W. 2002, ApJ, 567, L27
Markevitch, M., Govoni, F., Brunetti, G., & Jerius, D. 2005, ApJ, 627, 733
Markevitch, M., & Vikhlinin, A. 1997, ApJ, 491, 467
Markevitch, M., & Vikhlinin, A. 2007, Phys. Rep., 443, 1
Mitsuda, K., et al. 2007, PASJ, 59, S1
Mitsuda, K., et al. 2010, Proc. SPIE, 7732, 773211
Nagai, D., Vikhlinin, A., & Kravtsov, A. V. 2007, ApJ, 655, 98
Nishino, S., Fukazawa, Y., Hayashi, K., Nakazawa, K., & Tanaka, T. 2010, PASJ, 62, 9
Ota, N., et al. 2007, PASJ, 59, S351
Ozawa, M., et al. 2009, PASJ, 61, S1
Roettiger, K., Burns, J. O., & Pinkney, J. 1995, ApJ, 453, 634
Röttgering, H., Snellen, I., Miley, G., de Jong, J. P., Hanisch, R. J., & Perley, R. 1994, ApJ, 436, 654
Serlemitsos, P., et al. 2007, PASJ, 59, S9
Smith, R. K., Brickhouse, N. S., Liedahl, D. A., & Raymond, J. C. 2001, ApJ, 556, L91
Sugawara, C., Takizawa, M., & Nakazawa, K. 2009, PASJ, 61, 1293
Sun, M., Murray, S. S., Markevitch, M., & Vikhlinin, A. 2002, ApJ, 565, 867
Takahashi, T., et al. 2010, Proc. SPIE, 7732, 773202
Tamura, T., et al. 2009, ApJ, 705, L62
Tawa, N., et al. 2008, PASJ, 60, S11
Vikhlinin, A., Markevitch, M., & Murray, S. S. 2001, ApJ, 551, 160